Accepted Manuscript

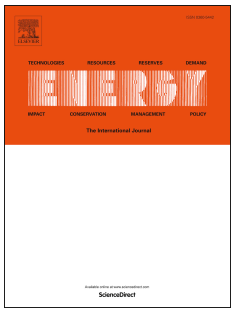

Novel battery state-of-health online estimation method using multiple health indicators and an extreme learning machine

Haihong Pan, Zhiqiang Lü, Huimin Wang, Haiyan Wei, Lin Chen

PII: S0360-5442(18)31285-4

DOI: 10.1016/j.energy.2018.06.220

Reference: EGY 13262

To appear in: *Energy*

Received Date: 18 November 2017

Revised Date: 28 June 2018

Accepted Date: 29 June 2018

Please cite this article as: Pan H, Lü Z, Wang H, Wei H, Chen L, Novel battery state-of-health online estimation method using multiple health indicators and an extreme learning machine, *Energy* (2018), doi: 10.1016/j.energy.2018.06.220.

Novel battery State-of-Health online estimation method using multiple health indicators and an Extreme Learning Machine

Haihong Pan[ab], Zhiqiang Lü[a], Huimin Wang[a], Haiyan Wei[a], Lin Chen[ab*]

a Department of Mechatronics Engineering, College of Mechanical Engineering, Guangxi University, Nanning, 530000, China

b Guangxi Key Laboratory of Manufacturing System & Advanced Manufacturing Technology, College of Mechanical Engineering, Guangxi University, Nanning, 530000, China

* Corresponding author: gxdxcl@163.com

Abstract

Battery health monitoring and management is critically important for electric vehicle performance and economy. This paper presents a multiple health indicators-based and machine learning-enabled state-of-health estimator for prognostics and health management. The multiple online health indicators without the influence of different loading profiles are used as effective signatures of the health estimator for effective quantification of capacity degradation. An extreme learning machine is introduced to capture the underlying correlation between the extracted health indicators and capacity degradation to improve the speed and accuracy of machine learning for online estimation. The proposed estimator is also compared to the traditional BP neural network. The associated results indicate that the maximum estimation error of the proposed health management strategy is less than 2.5 %, and it has better performance and faster speed than the BP neural network.

Keywords: Li-ion battery; Health indicator; State-of-Health; Extreme learning machine.

1. Introduction

As electric vehicles (EVs) have increased in popularity, research regarding battery management systems (BMSs) in the core technology of EVs has received a great deal of attention [1, 2]. Among the many functions of a BMS, the state-of-health (SoH) estimation of a battery (as a metric of battery aging) is one of the most significant factors in determining the time to replace a battery or in predicting driving mileage [3].

Methods for SoH estimation have been reviewed in Refs. [4-6]. These methods can mainly be classified into three categories: (1) direct measurement, (2) model-based approaches, and (3) data-driven approaches. In direct measurement, the batteries are fully charged and discharged to obtain the static battery capacity [5]. Beyond that, resistance measurements are also used to evaluate battery SoH [7, 8]. This is a kind of straightforward method, but there are limited application scenarios, such as a specialized laboratory environment. The main concept of the model-based SoH estimation is to connect online battery signals (terminal voltage, load current, and battery temperature) with battery SoH using a battery model. By measuring the battery online and using the signals as model inputs, a model can be used to calculate the battery states [9]. The main model-based approaches that have been reported can be further divided into two subgroups: (a) the electrochemical model and (b) the equivalent circuit (EC) model. The electrochemical model is established to mimic the growth of a solid electrolyte interface (SEI) in a Li-ion battery and to depict its effect on capacity degradation [10]. The electrochemistry-based model illustrates and elaborates a basic understanding of the spatiotemporal dynamics of electrochemical

reactions inside batteries [5]. Additionally, the electrochemical model provides theoretical and physical interpretations of some signs of battery aging. However, it is still inadequate for realistic applications because of the elusive partial differential equations. Also, the EC model focuses on a state/parameter observer design because the EC model parameters change, and the capacity decreases gradually as the batteries age [3]. Thus, mathematically, the battery SoH estimation problem is a parameter-monitoring problem. From control theory, it is known that key aspects include dual/joint extended Kalman filter, dual sliding-mode observation, recursive least squares, particle filter and so on. For example, Tran et al. [11] used dual extended Kalman filtering and an auto regressive exogenous model to detect changes in the battery parameters and to obtain the values of battery SoH. Kim et al. [12] presented a dual-sliding-mode observer, which consists of a fast-paced time-varying observer and a slow-paced time-varying observer. The two observers with different paces were used to estimate parameters and SoH, respectively. Shen et al. [13] identified the battery model parameters using the recursive least squares algorithm with a forgetting factor, and then the SoH was estimated using the relationship between battery capacity and identified parameters. Bi et al. [8] proposed a new genetic resampling particle filter for battery SoH dynamic estimation when the accuracy of the equivalent circuit model was not high. These observer-based techniques are online and closed-loop. Their effectiveness and adaptability are, however, sensitive to the robustness and credibility of the battery models [5]. Data-driven approaches are based on processing a great amount of multifaceted test data. These approaches have attracted increasing attention because of their flexibility and model-free characteristics. Some readily measurable data (e.g., terminal voltage, load current, historical state of charge (SoC), and operating temperature) or extracted

characteristic features are the inputs for “black-box” models for batteries. For instance, such “black box” models have included artificial neural networks, relevance vector machines, and sparse Bayesian predictive modeling. You et al. [3] proposed a data-driven approach based on neural networks to trace SoH using dynamic condition data while leveraging their historical distributions. For degradation modeling, Zhou et al. [14] extracted mean voltage falloff of lithium-ion batteries, and a regression equation was established to estimate capacity. Hu et al. [5] used the sparse Bayesian predictive modeling methodology to capture the underlying correspondence between capacity loss and sample entropy of short voltage sequence. The biggest problems are how to deal with the wide variety of test data using microprocessors and how to develop an accurate and robust algorithm that can provide great performance using online implementation [4].

Almost all of the methods mentioned above use some battery characteristic parameters, such as capacity or internal resistance, for the battery health indicator (HI) in battery degradation modeling [15]. The important reasons for this are that HI effectively simplifies the mass of measured data and reduces computation time. Therefore, positive and effective HI extraction has a significant influence on computational capacity and computation time. Thus far, some battery HI research has been focused on Li-ion battery prognostics. For example, the open circuit voltage (OCV) is an applicable HI for battery SoH [16]. However, accurate OCV measurement is time-consuming because a long rest time is required to reach a steady state for the battery [17]. Liu et al. [18, 19] reported that the time interval for the equal discharging voltage difference and the discharging voltage difference of an equal time interval in each discharge cycle could be used as HIs to quantify capacity degradation. However, a constant-current discharge is required to measure the time interval or the

discharge voltage difference. Hu et al. [5, 20] used sample entropy of a short terminal voltage sequence with a prognostic framework to manage battery health. Sample entropy is an advantageous computational tool to evaluate the predictability of a voltage series and to quantify the regularity of the voltage sequence. However, it is time-consuming to evaluate the sample entropy indicator [15], and the technique requires the same loading current profiles. Yang et al. [21] determined the relationship between coulombic efficiency evolution and capacity degradation to help develop battery degradation models and to estimate battery health states. However, to compute coulombic efficiency, the discharge capacity and charge capacity must be measured in the same cycle. Goh et al. [22] used the second-order differential voltage curve to describe the battery capacity; however, the reference voltage and input voltage curve must be measured under the same operating conditions.

Thus, it is crucial to seek an alternative online HI to quantify battery degradation. In this work, a novel kind of HI is extracted from the internal resistance online identification of Li-ion batteries. The goal is to achieve a simple and reliable technique for online battery degradation modeling and SoH estimation for EVs. Then, different correlation analyses were used for quantitative evaluation of the effectiveness of the relationship between capacity degradation and extracted HIs. In addition, the extreme learning machine (ELM), which is one of the most available techniques in machine learning that has a speed advantage and achieves satisfactory results [23, 24], was introduced to build a joint framework for online SoH estimation.

The two contributions of this study are as follows:

(1) Multiple HIs based on battery parameters of the Thevenin model were proposed for battery degradation modeling. An increase in ohmic internal resistance and an increase in polarized internal resistance were extracted as multiple HIs.

Theoretical deduction and experiment prove that these HIs are effective and free from the influence of different loading profiles.

(2) An online SoH estimation framework was developed. Using the extracted HIs, the ELM was introduced to train an offline learner to trace the capacity degradation and to provide model parameters for online SoH estimation. In addition, the performance of the proposed framework with ELM for SoH estimation is better than that of the BP neural network in terms of estimation accuracy and run time.

This paper is organized as follows: In Section 2, the test-setup, experimental design, and extracted online HIs are provided. In Section 3, the ELM is introduced, and the joint model-based ELM-oriented framework is developed for online SoH estimation. In Section 4, the results and discussions are presented. Finally, in section 5, the conclusions and future work are summarized on the basis of the results.

2. Li-ion battery test and HIs

In this work, the definition of SoH [4] is the percentage of the remaining battery capacity (C_{RBC}) and the initial battery capacity (C_{IBC}), as shown in Eq. (1). This calculation is also used to compare estimates obtained using different estimation methods.

$$SoH = \frac{C_{RBC}}{C_{IBC}} \times 100\,\% \tag{1}$$

where C_{RBC} (Ah) and C_{IBC} (Ah) are the available battery capacities in ampere hours, and these were measured according to specifications in the manufacturer's manual.

Battery cycling was implemented with a self-built battery test bench at multiple set temperatures and different loading profiles to explore capacity degradation. Such

experiments were also used to simulate actual driving situations of EVs.

2.1 Battery testing systems and schedule

The test bench that was used to acquire the required experimental data is shown in Fig. 1.

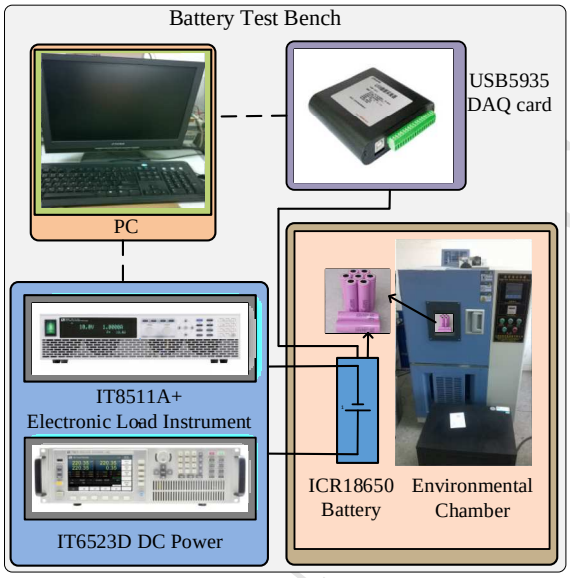

Fig. 1. *Schematic representation of the battery test bench.*

The test bench consists of a charger, ITECH IT6523D, ITECH electronic load IT8511 A+, Li-ion batteries, some custom switching circuitry (switching), a data acquisition system (DAQ), an environmental chamber, and a control computer. The major equipment parameters are listed in Table 1.

Table 1. *Major equipment parameters.*

Device name	Maximum Voltage (V)	Maximum current (A)
ITECH IT6523D	160 V± 0.2% full scale	120 A ± 0.2% full scale
IT8511 A+	120 V ± 0.0.05% full scale	30 A ± 0.1% full scale

The batteries used for this test were three lithium–nickel–manganese–cobalt (LiNMC) batteries (ICR18650-26F, from Samsung) with a graphite anode. Different batteries (No. 17 and No. 30 from the same batch of cells) were then used for three subsequent separate experiments to verify the generality of the proposed method used

in this study. The main specifications are given in Table 2.

Table 2. *Main specifications of the LiNMC cells.*

Nominal capacity (Ah)	Nominal voltage (V)	Charge cut-off voltage (V)	Discharge cut-off voltage (V)
2.60	3.70	4.20	2.75

All of the experiments were conducted in an environmental chamber, and the data acquisition frequency was 1 Hz. The entire apparatus and all of the equipment were operated at room temperature (25 °C with a tolerance of 2 °C).

The Li-ion batteries were run through three different operational profiles until 80% capacity loss was reached (considered to be the end of life). The three operational profiles were a capacity step, discharge step, and aging step, and these steps are described below.

First, charging was first conducted at a constant current (CC) of 1.30 A until the charge voltage reached a value of 4.20 V. Charging was then turned to a constant voltage mode until the charge current dropped to a value of 26 mA, and then the following three different operational profiles were implemented.

(1) **Capacity step**: Discharging was conducted at a CC of 0.52 A until the discharge voltage reached the predefined cutoff voltage of 2.75 V.

(2) **Discharge step**: Discharging was repeated using the New European Driving Cycle (NEDC) (Fig. 2 (a)) until the discharge voltage reached the predefined cutoff voltage of 2.75 V.

(3) **Aging step**: Discharging was repeated using pulsed discharge (Fig. 2 (b)) until the discharge voltage reached the predefined cutoff voltage of 2.75 V. This aging step was repeated 10 times.

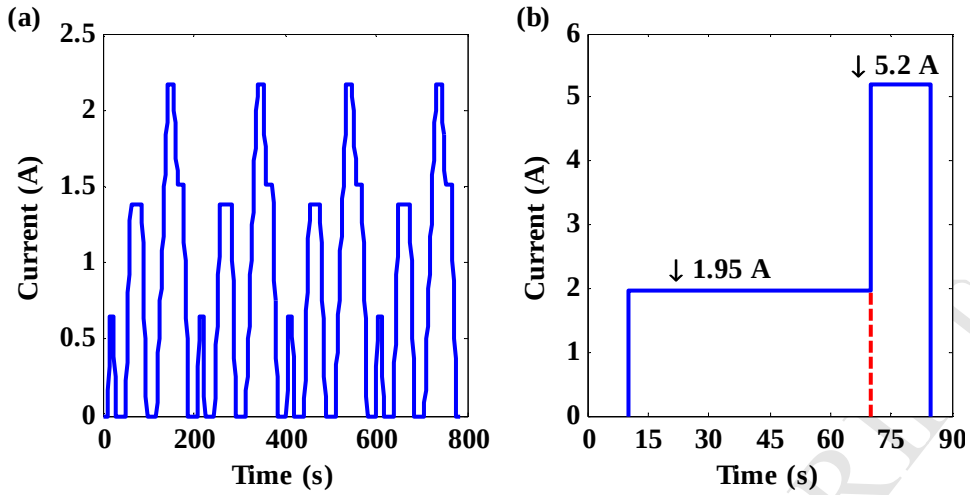

Fig. 2. *Current profiles for the batteries.*

For each 5% decline in the battery capacity, a characteristic experiment cycle was conducted, and this included different temperatures, different dynamic loading profiles, and OCV. Given the limits of the existing test-bed conditions, it should be noted that all of the experiments for No. 30 were at 35 ˚C. The capacity step and discharge step for No. 17 were at 25 ˚C, and the aging step was at 45 ˚C to accelerate aging. A range of experiments was conducted to investigate battery degradation at different temperatures.

2.2 Model parameter identification and evaluation

Generally, for Li-ion batteries, the parameters that can be readily detected and measured during operation are charging and discharging voltages, load current, and temperature. In Refs. [25, 26], the Thevenin model was used to model a battery, and the RLS algorithm was used for real-time parameter identification.

The robustness and accuracy of the Thevenin model and the RLS algorithm were validated using randomly selected dynamic loading profiles (Fig. 3).

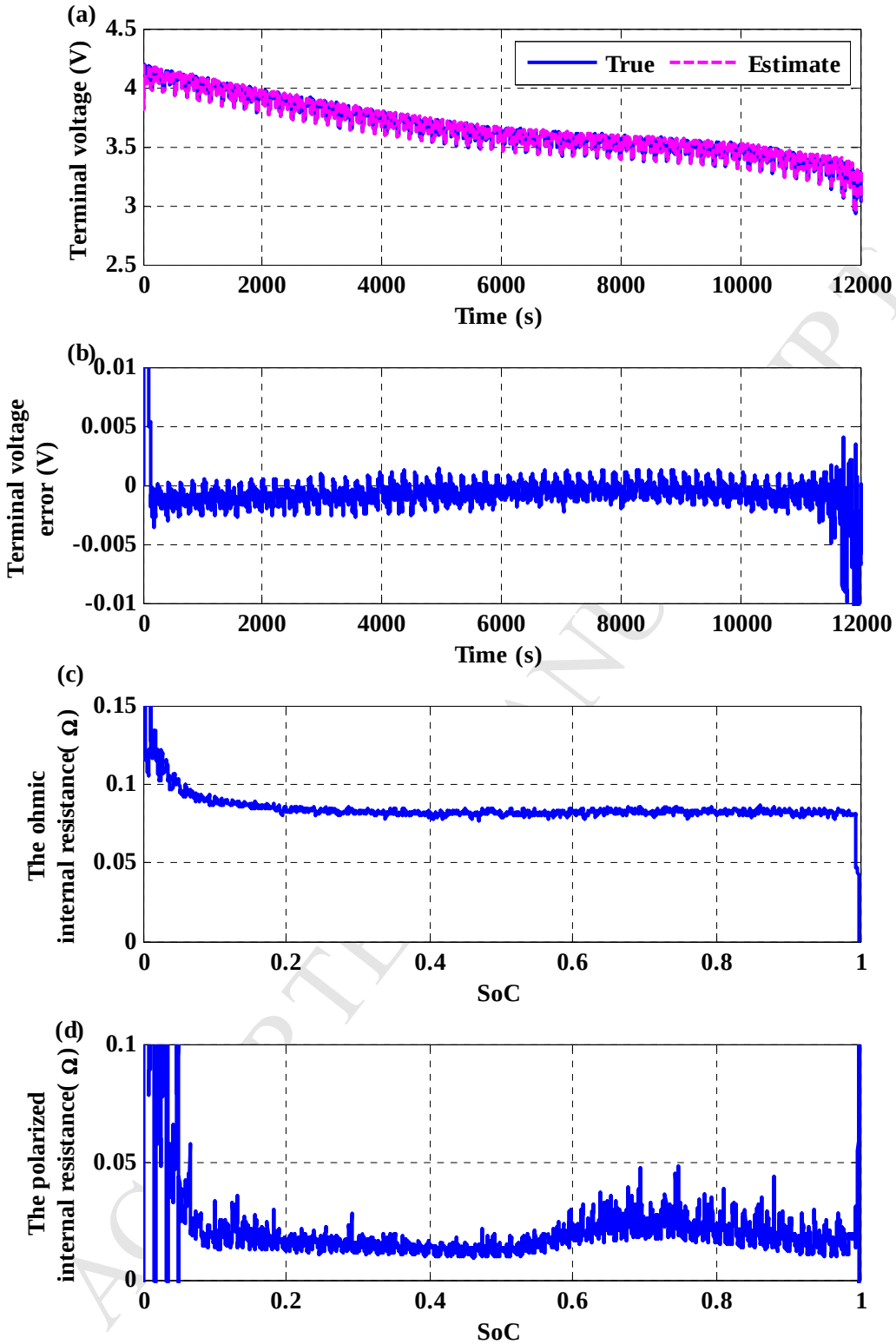

Fig. 3. *Validation results using the NEDC test: (a) terminal voltage estimation, (b) terminal voltage estimation error, (c) ohmic internal resistance, and (d) polarized internal resistance.*

Fig. 3 presents a comparison of experimental terminal voltage with the model simulation voltage and variations in ohmic internal resistance and polarized internal

resistance. There is good agreement between the model voltage and experimental voltage, and the maximum error is less than 5 mV, as shown in Fig. 3 (a) and (b). This suggests that the Thevenin model can be used for accurate tracking of the dynamic changes in the battery. However, the ohmic internal resistance remains invariably basic when the SoC is greater than or equal to 30 % (SoC is in the range of [0.3, 1]). The polarized internal resistance has a similar trend. In Ref. [27], Tulpule et al. reported that, in EVs, batteries are used until they are almost completely depleted (usually 95-25 % SoC), and then they are charged from external sources. Therefore, the values of ohmic internal resistance (R_0^i) and polarized internal resistance (R_1^i) for 80-30% SoC can be considered to be the values for certain aging stages. The expressions [28] for the ohmic internal resistance and polarized internal resistance are

$$\begin{aligned} R_0^i &= \frac{1}{n}\left(R_0\left(SoC=30\%\right)+\cdots R_0\left(SoC=80\%\right)\right) \\ R_1^i &= \frac{1}{n}\left(R_1\left(SoC=30\%\right)+\cdots R_1\left(SoC=80\%\right)\right) \end{aligned} \tag{2}$$

where $R_0\left(SoC\right)$ and $R_1\left(SoC\right)$ are the ohmic internal resistance and polarized internal resistance, respectively, at particular SoC. n is the number of elements in the sequence. The SoC is calculated using the Coulomb-counting method according to the definition of the method [25, 26].

Also, different conditions were implemented to assess the impact of different dynamic loading conditions on the accuracy of parameter identification. These different conditions included NEDC (mentioned above), the Urban Dynamometer Driving Schedule (UDDS, Fig. 4 (a)), and the Japanese 10.15 Mode Driving Schedule (JP1015, Fig. 4 (b)). As an example, for battery No. 30, the internal resistance under different loading conditions and different aging conditions (5%, 10%, 15%, and 20% of capacity degeneration) were calculated.

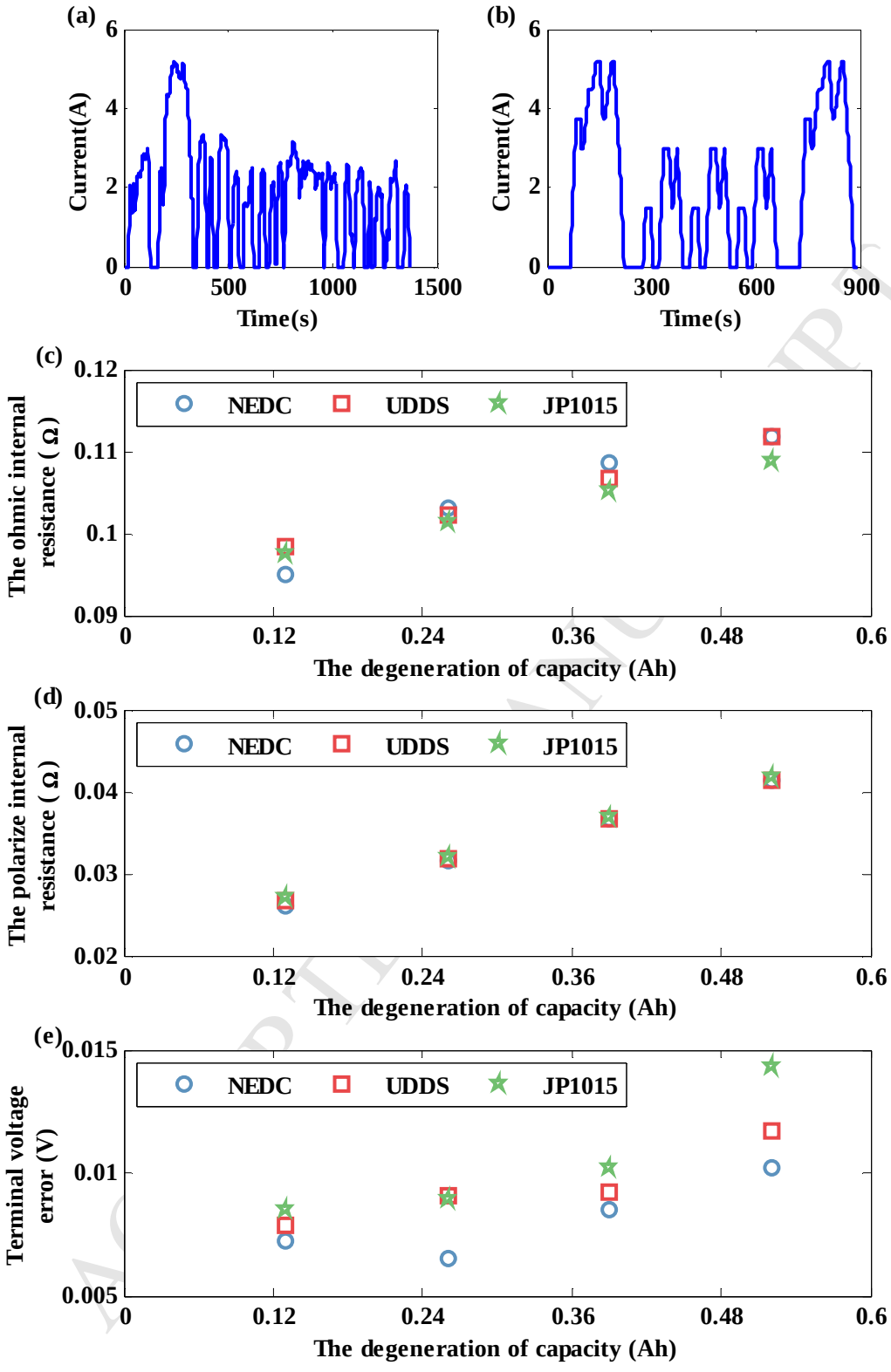

Fig. 4. *Various results for No.30 under different loading conditions and different aging conditions: (a) UDDS, (b) JP1015, (c) ohmic internal resistance, (d) polarized internal resistance, and (e) terminal voltage error.*

It is intuitive that, with aging time, different types of dynamic loading profiles

have minimal impact on the accuracy of parameter identification. The maximum error for the ohmic internal resistance is no more than 3mΩ, and the maximum error for the polarized internal resistance is no more than 1mΩ. The maximum error for the combined internal resistance is about 3%. Additionally, all of the terminal voltage errors are less than 1% of the discharge cut-off voltage (27.5 mV). There are good reasons to suggest that the Thevenin model and RLS algorithm have sufficient accuracy to identify the model parameters without the influence of different loading profiles. Furthermore, two-way ANOVA was also used to assess the significance of the impact of loading profiles and aging conditions on the identification results. The ANOVA results are shown in Table 3 and Table 4.

Table 3. *Ohmic internal resistance results of two-way ANOVA.*

Source	SS	Df	MS	F
Aging conditions	0.00032	3	0.00011	47
Loading profiles	0.00001	2	0	1.31
Error	0.00001	6	0	
Total	0.00034	11		

Table 4. *Polarized internal resistance results of two-way ANOVA.*

Source	SS	df	MS	F
Aging conditions	0.00037	3	0.00012	4608.92
Loading profiles	0	2	0	13.3
Error	0	6	0	
Total	0.00037	11		

At the 0.005 significance level, the values of $F_{0.005}(3,6)$ and $F_{0.005}(2,6)$ are 12.92 and 14.54, respectively. For the different aging conditions, both of the computed F values are greater than the look-up table values, and this suggests that the

different aging conditions have a significant impact on battery model parameters. In contrast, both of the computed F values are less than the look-up table values for the corresponding loading profiles; this indicates that the different loading profiles have no significant impact on the battery model parameters.

Therefore, the Thevenin model and RLS with NEDC can be used to obtain the real-time ohmic internal resistance and polarized internal resistance over the whole aging process. The measured remaining battery capacity (C_{RBC}), computational ohmic internal resistance (R_0^i), and polarized internal resistance (R_1^i) of the LiNMC cells over the whole aging process are shown in Fig. 5.

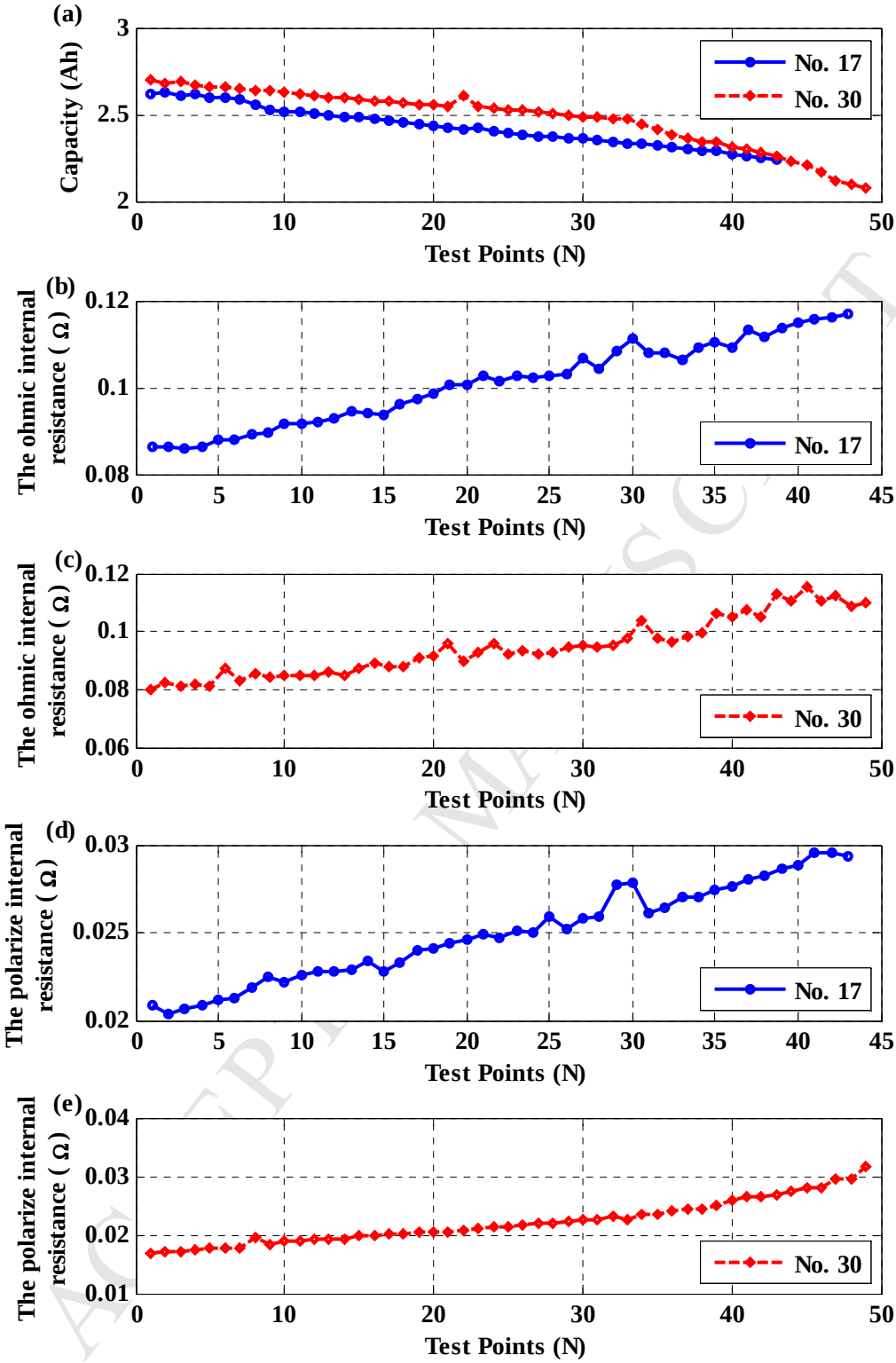

Fig. 5. *Capacity and resistance evolution during aging: (a) capacity evolution, (b) ohmic internal resistance evolution of No.17, (c) ohmic internal resistance evolution of No.30, (d) polarized internal resistance evolution of No.17, and (e) polarized internal resistance evolution of No.30.*

The capacities decline gradually, and the ohmic internal resistance and polarized

internal resistance each increase in a nonlinear and non-Gaussian trend. The decreasing or increasing trends in the same parameters for different batteries are similar to a certain degree, and thus, these similar trends may be considered as beneficial signatures for degradation modeling.

2.3 HI extraction

As mentioned earlier, there is an urgent need to find an alternative HI for the operating parameters of Li-ion batteries to quantify degradation. The battery parameters that are easily detected and measured include terminal voltage, load current, and environmental temperature. The ohmic internal resistance and polarized internal resistance can be effectively calculated according to Eq.(2) on the basis of the measured data, Thevenin model, and RLS algorithm.

Furthermore, according to Ref. [29], there is a linear relationship between battery capacity degradation and battery impedance, and according to Ref. [30], high temperature has only a small effect on resistance. In contrast, low temperature has a large effect on resistance. Usually, the boundary temperature is 20 °C. Temperature has a large impact on resistance; however, at the same aging stages for the same temperature, it has a relatively small impact on increasing resistance. Therefore, an increase in the ohmic internal resistance and an increase in the polarized internal resistance can be used to quantify the battery capacity degradation in each discharging cycle. In particular, an increase in the ohmic internal resistance (ΔR_0^i) and an increase in the polarized internal resistance (ΔR_1^i) are two HIs that can be used for SoH estimation. The expressions [28] for HIs extraction are

$$\Delta R_0^i = R_0^i - R_0^1 \tag{3}$$

$$\Delta R_1^i = R_1^i - R_1^1$$

where R_0^1 and R_1^1 are the initial ohmic internal resistance and polarized internal resistance, respectively.

The HI-capacity degradation results are shown in Fig. 6 to observe the relationship between the extracted HIs and capacity degradation.

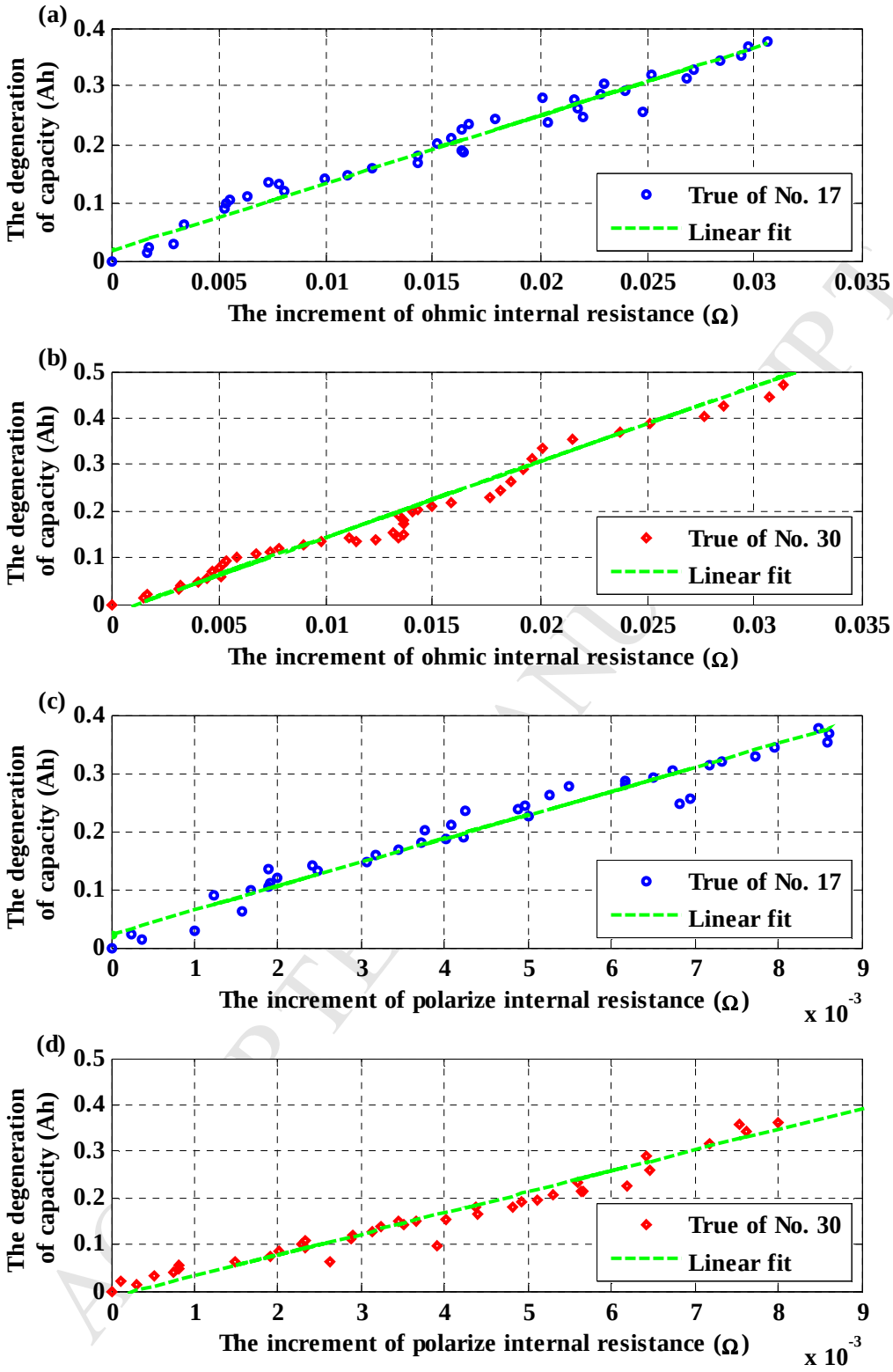

Fig. 6. *Capacity degradation and HIs: (a) capacity degradation and incremental increase in ohmic internal resistance for No.17, (b) capacity degradation and incremental increase in ohmic internal resistance for No.30, (c) capacity degradation and incremental increase in polarized internal resistance for No.17, and (d) capacity degradation and incremental increase in polarized internal*

resistance for No.30.

There is a good linear relationship between the extracted HIs and capacity degradation. Only qualitative information can be obtained from Fig. 6; additional parameters are required to elaborate further on the relationship between HIs and capacity degradation. The detailed linear fit results are shown in Table 5.

Table 5. *HI performance evaluation results.*

HIs	Index	No.17	No.30
ΔR_0^i	RMSE	0.0181	0.0203
	R^2	0.9749	0.9750
ΔR_1^i	RMSE	0.0203	0.0182
	R^2	0.9685	0.9799

As shown in Table 5, the values of RMSE and R^2 are approximately 0.02 and 0.97, respectively, and these values indicate a good statistical fit. The results shown in Table 5 also indicate that there is good similarity between the HIs and capacity degradation.

2.4 Correlation analysis

The Pearson correlation (r_P) and Spearman rank correlation (r_S) between the HI series and capacity degradation series were calculated to obtain quantitative evaluations of the correlation between the HIs and the capacity degradation. The Pearson and Spearman rank correlations are computed as [15]

$$r_P = \frac{E(XY) - E(X)E(Y)}{\sqrt{E(X^2) - E(Y^2)}\sqrt{E(Y^2) - E^2(Y)}}$$
$$r_S = \frac{\sum_i (X_i - \bar{X})(Y_i - \bar{Y})}{\sqrt{\sum_i (X_i - \bar{X})^2}\sqrt{\sum_i (Y_i - \bar{Y})^2}} \quad (4)$$

where X and Y are known series.

Pearson correlation analysis was used for a quantitative validation of the linear relationship between the extracted HIs and capacity degradation. The value of r_P is between -1 and +1, and a greater absolute value of r_P indicates that there is a better linear relationship between HI and capacity degradation. If the value of r_P is 0, there is no correlation between the two variables. Additionally, Spearman rank correlation analysis is a nonparametric way to assess the strict monotonic relationship between HI and capacity degradation. Similarly, the value of r_S is between -1 and +1. If $r_S > 0$, there is a strong positive correlation between HI and capacity degradation; otherwise there is a negative correlation [15]. The correlation analysis results for the two batteries are shown in Table 6.

Table 6. *Correlation analysis.*

HI	Method	No.17	No.30
ΔR_0^i	Pearson	0.9874	0.9529
	Spearman	0.9894	0.9735
ΔR_1^i	Pearson	0.9841	0.9909
	Spearman	0.9885	0.9913

Both of the two Pearson correlation coefficients are greater than 0.95 and are approximately 1, and this implies that the correlations between the extracted HIs and capacity degradation are nearly linear. Although the Spearman correlation analysis shows that the relationship between the extracted HIs and capacity degradation is not strictly monotonic, the values of ΔR_0^i and ΔR_1^i are accurate enough to be used as new HIs.

From the analysis and calculations above, a conclusion can be drawn that the two extracted HIs have a strong linear correlation with the capacity degradation and that this correlation is both qualitative and quantitative. Also, the HIs are reasonable

enough to replace capacity for quantifying battery degradation.

3. ELM-oriented SoH estimation

In this section, the fundamentals of the ELM are elaborated in detail. The online framework for SoH estimation is then built on the basis of the extracted HIs and ELM theory.

3.1 ELM theory

The ELM was proposed by Huang et al. [24] as a unique way of building a single hidden layer feed forward neural network (SLFN) [23]. The ELM has attracted extensive attention because of its unique ability to learn extremely quickly. The main feature of ELM is the random initialization of the input weights and biases, and thus, it is only necessary to optimize the weights that connect the output layer. ELM surpasses many time-consuming algorithms such as back propagation (BP) algorithms.

Consider a data set containing N training samples $\{(\mathbf{x}_i, y_i)\}_{i=1}^{N}$, for which the input is $\mathbf{x}_i \in R^n$ and the corresponding desired output is $y_i \in R^n$ under the assumption that the model perfectly describes the relationship between $\mathbf{x}_i$ and y_i. Suppose that ELM with L hidden nodes can be described as [24]

$$\sum_{i=1}^{L} \beta_i g(\boldsymbol{\omega}_i \cdot \mathbf{x}_j + b_i) = y_j, \quad j = 1,2,\ldots,N \tag{5}$$

where $\boldsymbol{\omega}_i = [\omega_{i1}, \omega_{i2}, \ldots \omega_{in}]^T$ is a randomly chosen input weight vector connecting the ith hidden neuron and the input neurons. b_i denotes the randomly chosen bias of the ith hidden node, and β_i is the weight that connects the ith hidden neuron

348 and the output neuron. $\boldsymbol{\omega}_i \cdot \mathbf{x}_j$ represents the inner product of $\boldsymbol{\omega}_i$ and $\boldsymbol{x}_j$, and the
349 output node is chosen to be linear. The above *N* equations can be compactly written as
350 a linear system [24]:

$$\mathbf{H}\beta = \mathbf{y} \tag{6}$$

351 where $\mathbf{H}(\boldsymbol{\omega}_1, \ldots \boldsymbol{\omega}_L, \mathbf{x}_1, \ldots \mathbf{x}_N, b_1, \ldots b_L) = \begin{bmatrix} g(\boldsymbol{\omega}_1 \cdot \mathbf{x}_1 + b_1) & \cdots & g(\boldsymbol{\omega}_L \cdot \mathbf{x}_1 + b_L) \\ \vdots & \cdots & \vdots \\ g(\boldsymbol{\omega}_1 \cdot \mathbf{x}_N + b_1) & \cdots & g(\boldsymbol{\omega}_L \cdot \mathbf{x}_N + b_L) \end{bmatrix}$,

352 $\beta = [\beta_1, \beta_2, \ldots, \beta_L]^T$, and $\boldsymbol{y} = [y_1, y_2, \ldots, y_N]^T$.

353 All of the parameters are known except for the output weight (β) in the ELM
354 model. Thus, the purpose is how to find the solution of the output weight quickly
355 according to Eq. (6). The optimal solution has the form [24]

$$\hat{\beta} = \mathbf{H}^{+}\mathbf{y} \tag{7}$$

356 where $\mathbf{H}^{+}$ is the Moore–Penrose generalized inverse of the hidden layer output
357 matrix $\mathbf{H}$. Because the number of training samples is usually greater than the number
358 of hidden nodes ($N > L$), least squares can be used to rewrite Eq. (8) as [23]:

$$\hat{\beta} = (\mathbf{H}^T\mathbf{H})^{-1}\mathbf{H}^T\mathbf{y} \tag{8}$$

359 An ELM, whose overall structure contains some neurons and their internal
360 connections, was developed to mathematically mimic the genetic activity of the brain.
361 A simplified structure to depict this concept is shown in Fig. 7.

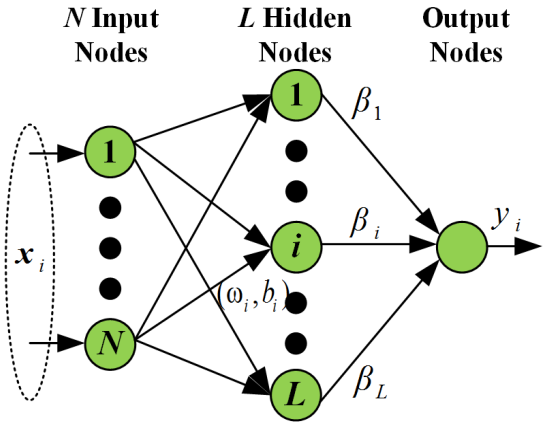

Fig. 7. *Structure of the ELM.*

3.2 Battery SoH estimator

The overall SoH estimation framework mainly contains two parts to identify the distribution differences and to estimate the SoH online. The two parts are shown in Fig. 8: (1) the offline learner that trains an ELM estimation model from some collected data sets and provides the model parameters to the BMS and (2) the online SoH estimator of the BMS that receives online signals from the battery and traces the capacity degradation. The capacity degradation is further used to compute the remaining battery capacity (C_{RBC}) and SoH according to Eq. (1).

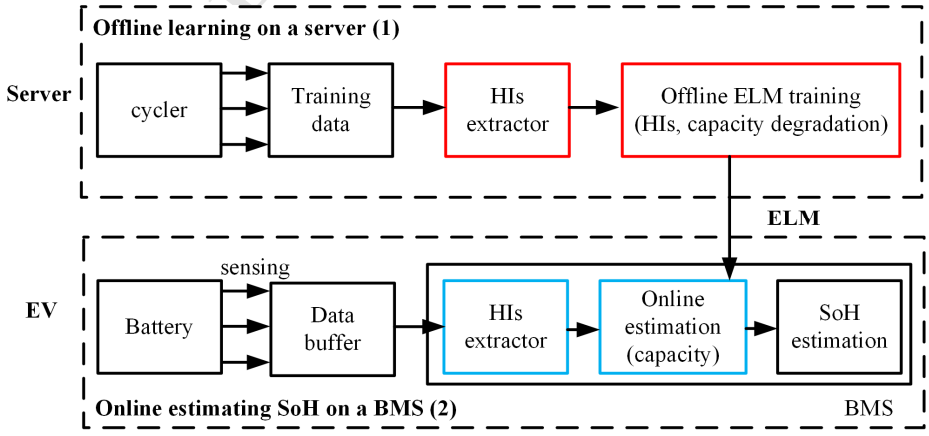

Fig. 8. *Online framework for SoH estimation (top: offline learning; bottom: online estimation).*

The SoH estimator is first calibrated offline using representative aging data sets of a reference battery, and then it is deployed for use with another battery. Because the

input (the increase in the ohmic internal resistance (ΔR_0^i) and the increase in the polarized internal resistance (ΔR_1^i)) calculation is highly efficient, the capacity degradation estimate can be obtained rapidly. This scenario is advantageous for estimating the battery capacity of an actual EV, in which a vehicle prototype can be used to establish the capacity estimator that acts as a standard for monitoring the health of a user's vehicle.

A comparison with the traditional BP neural network counterpart was conducted [24] to further verify the effectiveness of the ELM-oriented SoH estimation. The topology of the BP neural network that was used is detailed in Ref. [31]. The SoH framework that is based on the BP neural network is similar to that of ELM except that the machine learning algorithm is replaced by the BP algorithm. Each of the methods uses identical Sigmoid functions and training/validation data, and both of the hidden notes of the ELM and BP neural network are 20.

4. Results and discussion

This section describes the evaluation of the estimation results using the estimator described in Section 3.2. The test data for battery cells No. 17 and No. 30 were selected from the same batch of cells to demonstrate the performance of the developed framework for online SoH estimation. In addition, the data of No. 30 were used for offline learning, and the data of No. 17 were used for online SoH estimation. Also, to compare the effectiveness of the ELM-oriented SoH estimation, the traditional BP neural network was used to estimate the SoH using the same HIs.

In the simulations throughout this article, the software and hardware platform configuration information are as follows: Desktop, Intel core i3-4150 3.5G CPU, 8G DDR3 RAM, Windows 7, MATLAB R2014a.

4.1 Capacity degradation estimation

It is important and useful to investigate the robustness of the ELM and BP neural network for online SoH estimation. An increase in the ohmic internal resistance (ΔR_0^i) and an increase in the polarized internal resistance (ΔR_1^i) can be efficiently calculated using the Thevenin model and RLS [25, 26]. The estimators can then be used to indicate the capacity degradation. The estimation results that were obtained using the ELM and BP neural network are shown in Fig. 9.

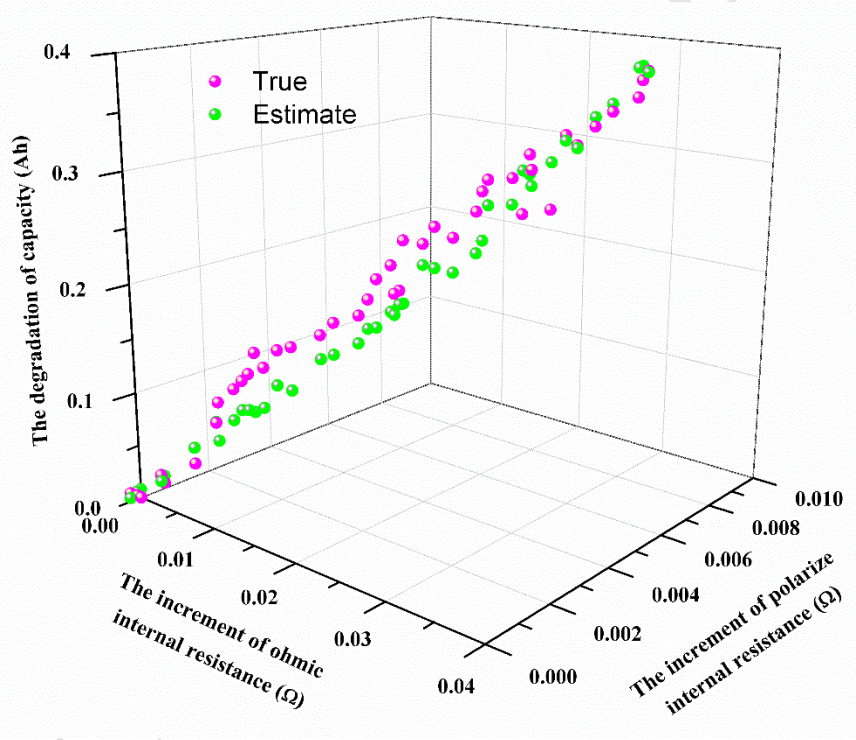

(a) Measured and estimated capacity degradation using the ELM.

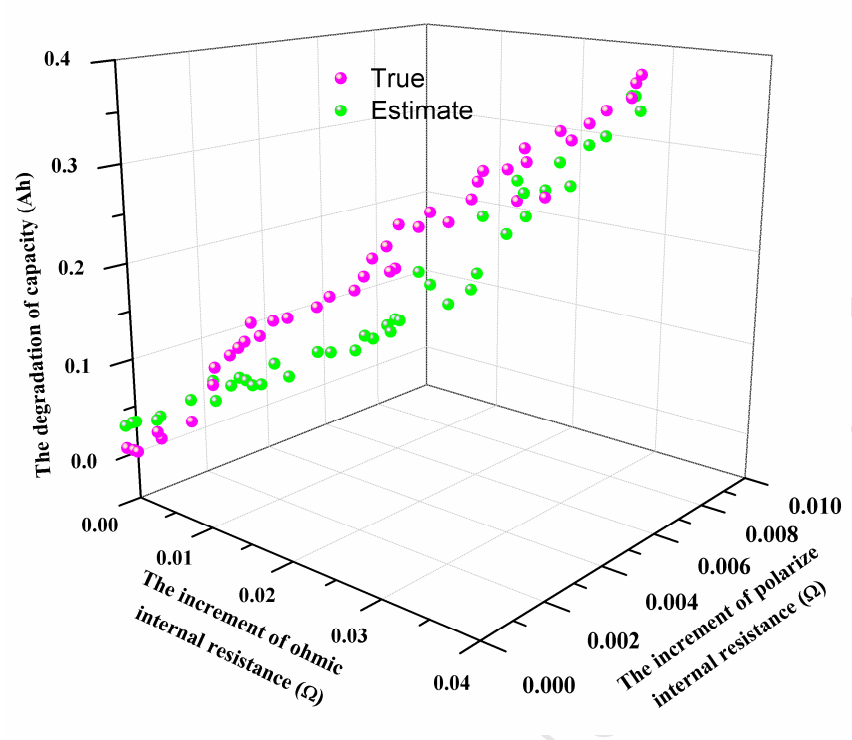

409

410 *(b) Measured and estimated capacity degradation using the BP neural network.*

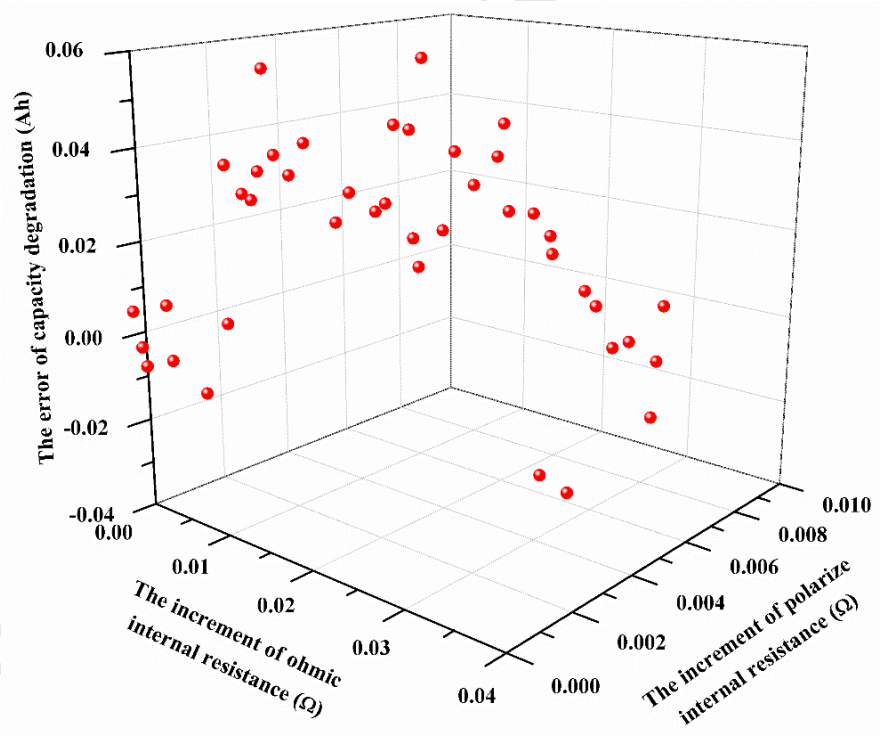

411

412 *(c) Capacity degradation error using the ELM.*

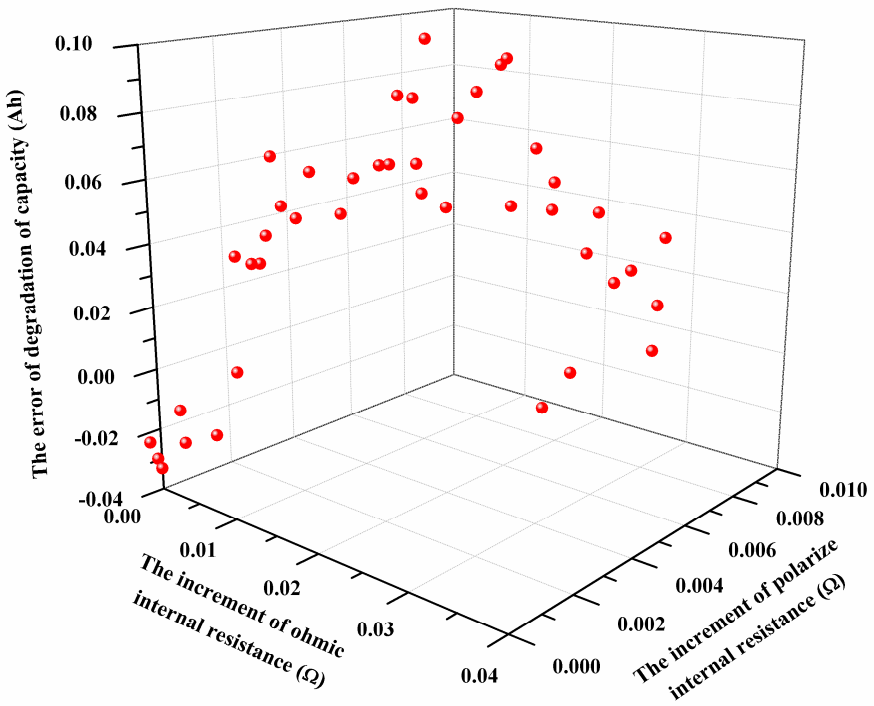

413

414 *(d) Capacity degradation error using the BP neural network.*

415 ***Fig. 9*** *Comparison of capacity degradation estimation for No. 17.*

416 As seen in Fig. 9 (a) and (b), as ohmic internal resistance and polarized internal
417 resistance increase, battery capacity degradation also increases. The estimation
418 capacity degradation can trace the dynamic capacity degradation trajectories; however,
419 the difference between the estimation capacity degradation and true capacity
420 degradation using the ELM (Fig. 9 (a) is better than that using the BP neural network
421 (Fig. 9 (b)). The maximum estimation error of the ELM is no more than 0.06 Ah,
422 which is less than the 0.10 Ah of the BP neural network, as shown in Fig. 9 (c) and (d),
423 respectively. The estimation errors of battery capacity degradation of the two different
424 methods have slightly different trajectories, and the error distribution of the ELM is
425 more narrow than that of the BP neural network.

426 The detailed statistical analysis based on the online estimation battery capacity
427 degradation results is shown in Table 7 and includes the maximum error, mean
428 absolute error (MAE), and the root mean square error (RMSE).

Table 7. *Comparison of capacity degradation determined using ELM and the BP neural network.*

Methods	Maximum	MAE	RMSE
ELM	0.0581	0.0238	0.0280
BP	0.1011	0.0456	0.0528

Overall, as the cell capacity decreased, the values of the HIs increased. It is clear that the capacity degradation estimates obtained using the ELM and neural network can be used to trace the real capacity degradation that is determined on the basis of the extracted HIs. The maximum capacity degradation error of the ELM is 0.0581 Ah, and this is less than the error of the BP neural network (0.1011 Ah). MAE of the estimated capacity degradation of ELM is 0.0238 Ah, and this is less than the error of the BP neural network (0.0456 Ah). Statistically, MAE is a measure of the difference between the estimated and real values of capacity degradation. The MAE results show that, overall, the ELM has smaller capacity degradation errors than the BP neural network. Also, the RMSE of ELM is 0.0280 Ah, which is less than that of the BP neural network (0.0528 Ah). In general, RMSE is a frequently used measure for the differences between the predicted values using an estimator and the observed actual values. The RMSE results show that the capacity degradation estimated using the ELM is better than that obtained using the BP neural network. Also, the estimation errors based on the ELM show good randomness. In terms of system identification, the randomness, in turn, verifies the validity and good general ability of the ELM-oriented SoH estimator. Therefore, based on this multifaceted comparison of capacity degradation, the ELM estimation performance is better than that of the traditional BP neural network.

4.2 SoH estimation

The remaining battery capacity (C_{RBC}) can be further estimated on the basis of

the capacity degradation as described in Section 4.1, and the results are shown in Fig. 10.

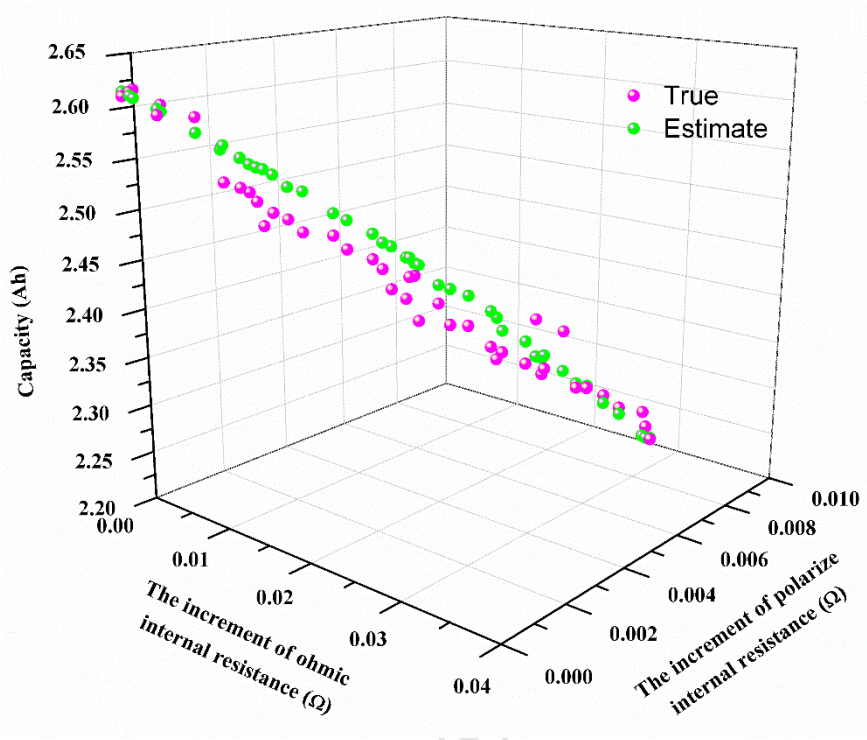

(a) Capacity estimation using the ELM.

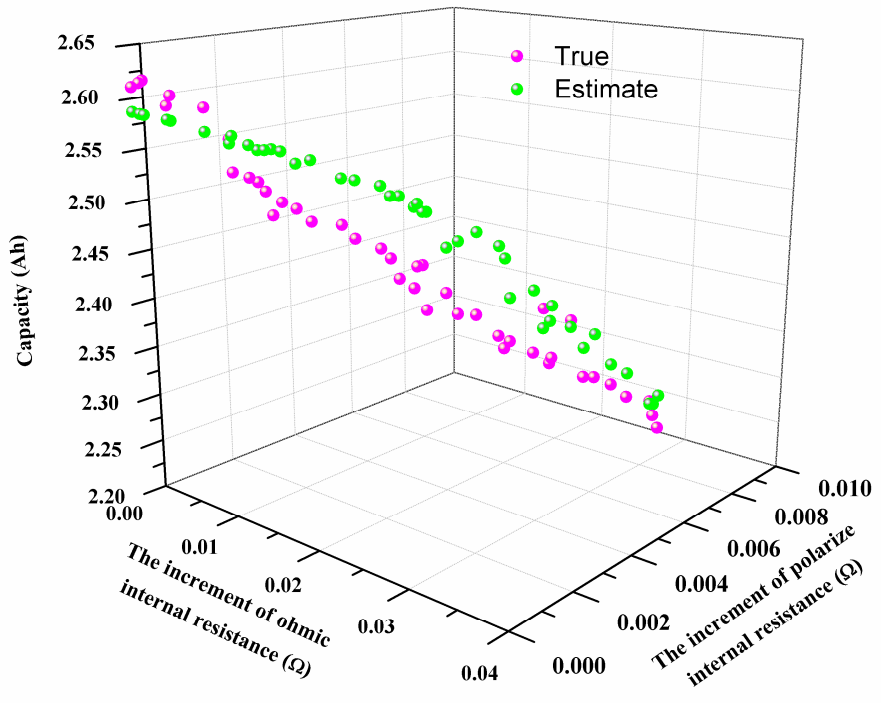

(b) Capacity estimation using the BP neural network.

Fig. 10. *Comparison of capacity estimation for No. 17.*

458 Similar to Fig. 9, Fig. 10 shows that as the health factors increase, battery
459 capacity degrades. The trajectories between estimated capacity and true capacity have
460 a high degree of overlap, and this suggests that the battery capacity estimated by the
461 two methods have sufficiently high accuracy. However, from the differences between
462 the two figures, the accuracy of the ELM is higher than that of the BP neural network
463 (Fig. 10). Therefore, the accurate capacity estimation lays the data foundation for
464 estimating the health status.

465 For a schematic illustration of how our proposed approach works, the value of
466 SoH can be computed on the basis of the capacity estimation and the SoH definition
467 (Eq.(1)). The probabilistic distribution and SoH error statistics were calculated to
468 show more clearly the validity and robustness of the estimators, and the results are
469 shown in Fig. 11.

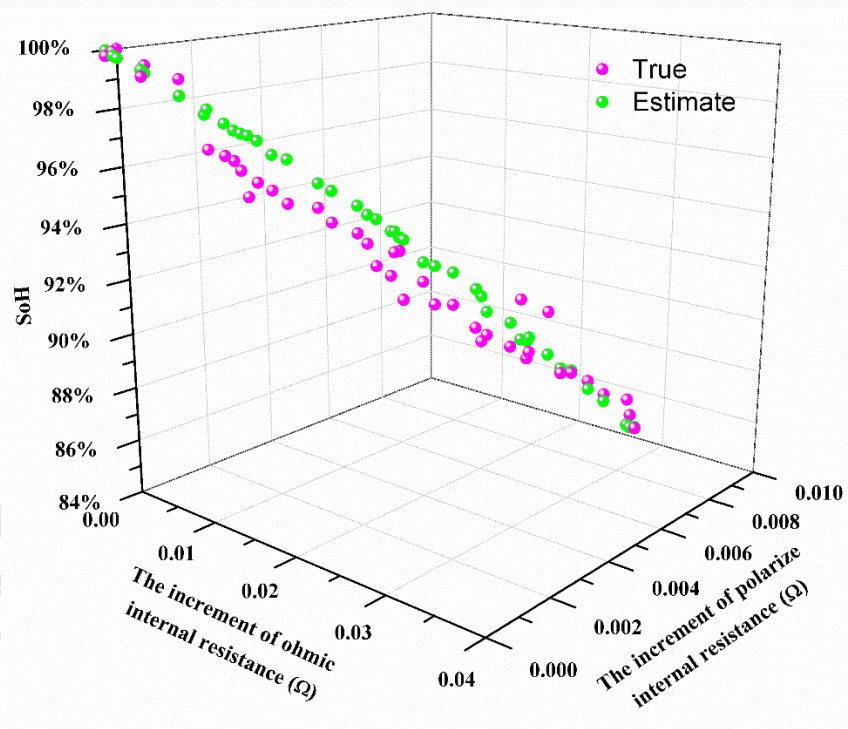

470

471 *(a) SoH estimation using the ELM.*

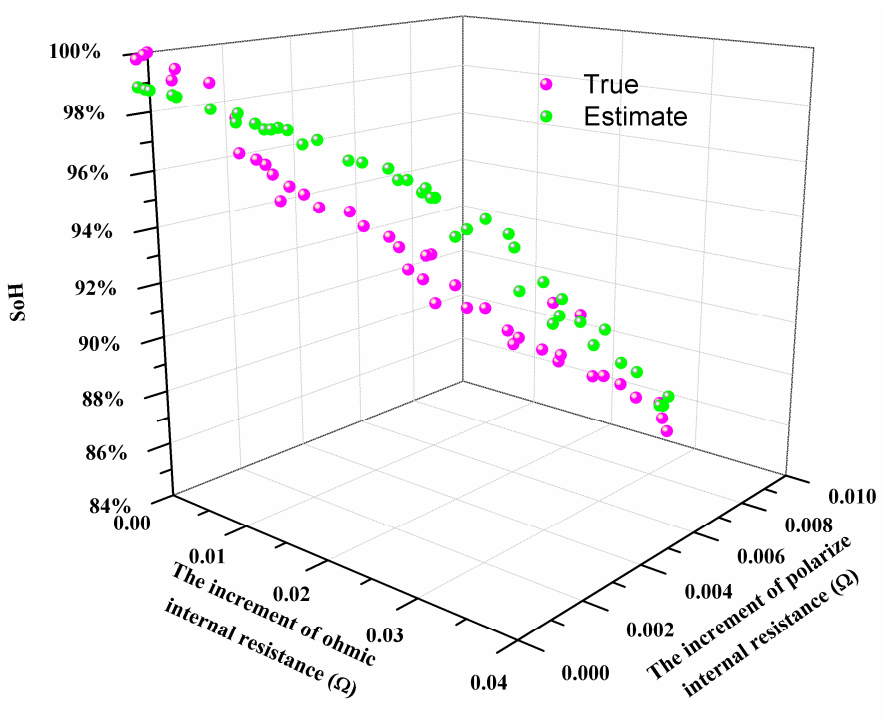

(b) SoH estimation using the BP neural network.

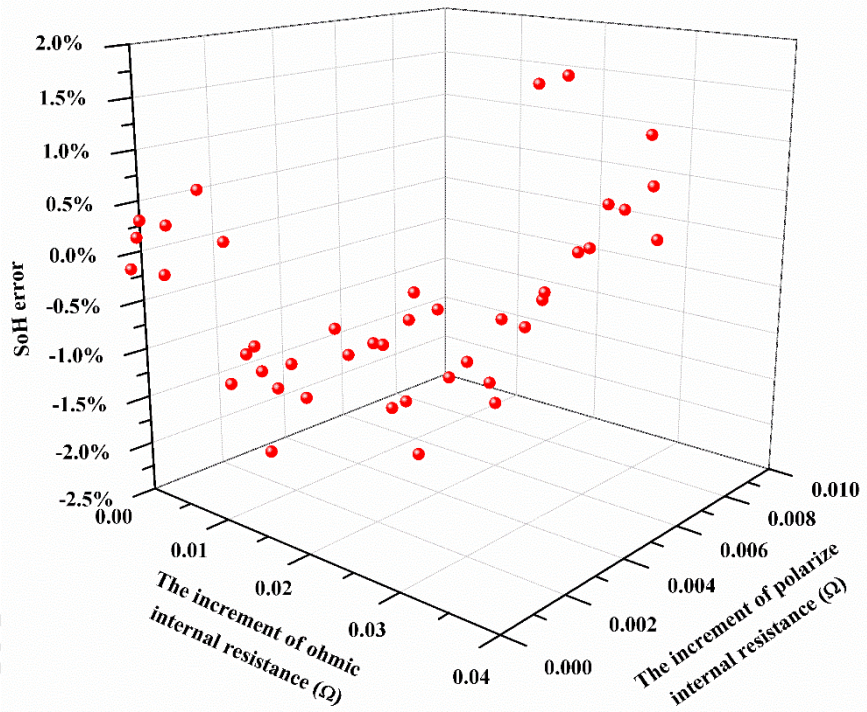

(c) SoH error using the ELM.

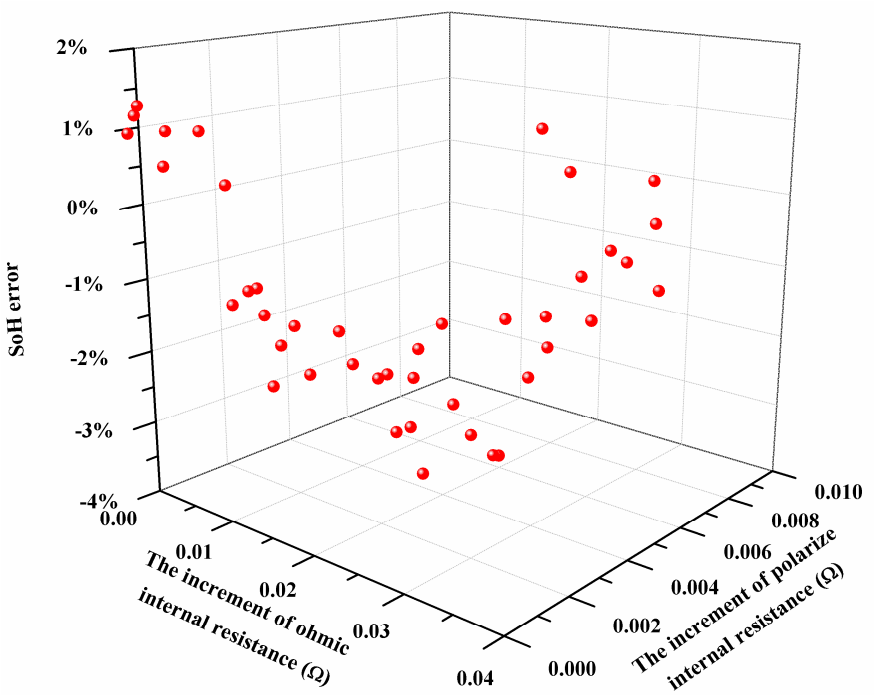

476

477 *(d) SoH error using the BP neural network.*

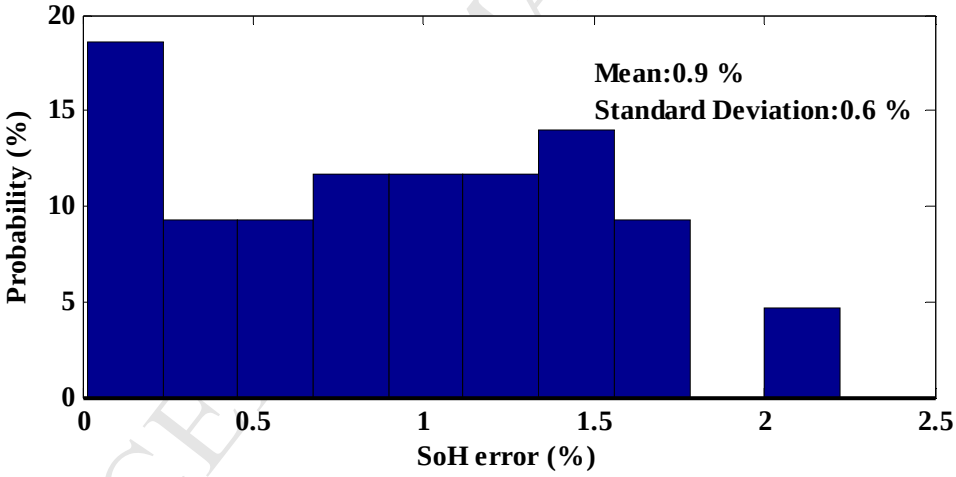

478

479 *(e) Distribution of the relative capacity errors using the ELM.*

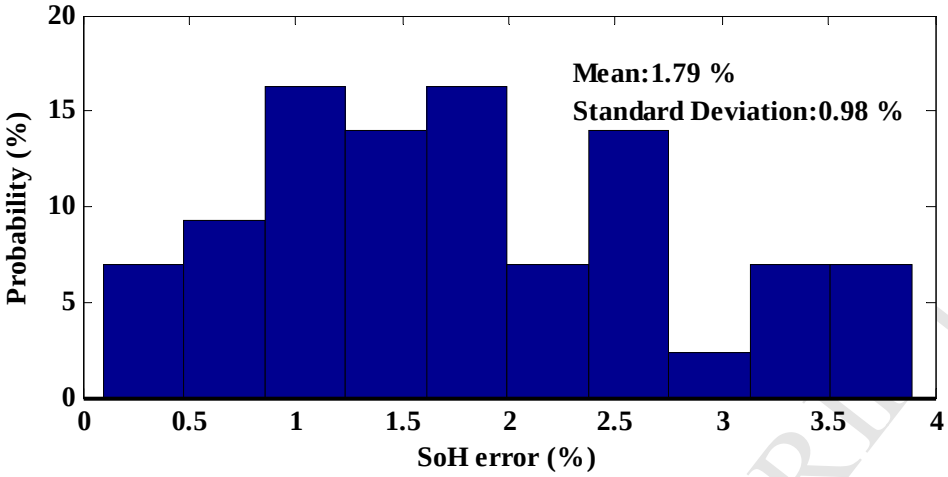

(f) Distribution of the relative capacity errors using the BP neural network.

Fig. 11. *Comparison of SoH estimation results for No.17.*

SoH gradually decreases with an increase in HIs, and both the ELM and BP neural network can estimate the SoH with high accuracy, as seen in Fig. 11 (a) and (b). Similarly, the values of SoH estimated using the ELM can track battery degradation trajectory with greater accuracy than the BP neural network can. The SoH estimation errors of each of the two methods were calculated. The margin of SoH errors of the ELM is in the region of [-2.5%, 2%] (Fig. 11 c), but the error range of the BP neural network is [-4.0%, 2%] (Fig. 11 d). The estimation errors of SoH provide good evidence that the ELM has higher estimation accuracy than the BP neural network. To show more clearly the validity and robustness of the estimators, the probabilistic distribution of SoH errors was calculated, and the results are shown in Fig. 11 (e) and (f). The probabilistic distribution results indicate that, from particular perspectives, the errors for the ELM are better than those of the BP neural network. The mean and standard deviation of the estimation errors for the ELM are 0.9% and 0.6%, respectively. For the BP neural network, these errors are 1.79% and 0.98%, which are obviously higher than those for the ELM. Both the ELM and BP neural network can achieve accurate online SoH estimation because of the effectiveness of the multiple

499 HIs. However, the ELM performs better than BP neural network because it has good
500 generalized performance.

501 Furthermore, to contrast the performance of the SoH estimation errors between
502 the ELM and BP neural network, the maximum error, MAE, and RMSE were used to
503 analyze the characteristics of the the ELM and BP neural network, and the results are
504 shown in Table 8.

505 ***Table 8.*** *Comparison of SoH estimation between the ELM and BP neural network.*

Methods	Maximum	MAE	RMSE
ELM	2.22 %	1.72 %	0.0109
BP	3.89 %	1.79 %	0.0203

506 The estimated SoH and true SoH show a high degree of coincidence. Although
507 the degradation trajectories vary in a nonlinear and non-Gaussian trend (Fig. 5), the
508 results consistently trace very well. It must be proven that the estimation made using
509 the ELM has better robustness and effectiveness with respect to the SoH estimation
510 than the BP neural network has. In particular, the ELM has good performance with a
511 maximum error of 2.22%, MAE of 1.72%, and RMSE of 0.0109. In contrast, the BP
512 neural network has slightly worse performance with a maximum error of 3.89%,
513 MAE of 1.79%, and RMSE of 0.0203. Furthermore, the time required to make the
514 estimations using the ELM and BP neural network are 0.0136 s and 0.3420 s,
515 respectively; the time for the ELM is an order of magnitude higher than that for the
516 BP neural network. The smaller time results obtained using the ELM suggest that it
517 performs better for an online SoH estimation than the traditional BP neural network,
518 and the two times indicate the speediness of the estimator based on the ELM.
519 Furthermore, compared to Ref. [3], the effective HIs can avoid large amounts of data
520 (terminal voltage, load current, and temperature) input into the neural network
521 structure. Also, the ELM has a simpler structure, faster speed, and higher accuracy

than the neural networks that were used and reported in Ref. [3].

4.3 Discussion

The good performances reported in this work suggest that capacity degradation is related to the extracted HIs over cycling because they follow a similar growth trend. The correlations between capacity degradation and the extracted HIs have also been proven by multiple correlation analyses, including Pearson correlation and Spearman rank correlation. The correlation analysis results indicate that capacity degradation and the extracted HIs most likely result from the same mechanistic origins, such as the loss of active material and electrochemical reactions. HIs can be used for accurate identification of battery capacity degradation. The primary possible reasons for this are as follows: SEI formation usually causes predominant aging mechanisms [4, 32], and the SEI develops over time, which causes a continuous loss of lithium ions [33]. As a result, this loss of available lithium ions leads to a significant increase in impedance and capacity degradation [4]. Also, lithium metal plating contributes to accelerated aging, which causes capacity fading. Lithium plating results in less active material; thus, the battery capacity decreases, and the battery impedance increases. The essential reason for battery performance degradation is that electrochemical reactions inside the battery reduce the amount of lithium ions and electrolyte, and this increases the battery impedance and reduces the battery capacity. Therefore, the extracted HIs can be used to quantify capacity degradation. In addition, the HIs can be efficiently calculated for realistic EV operation.

In terms of machine learning, the ELM also performs better than the BP neural network. From a mathematical point of view, the traditional BP neural network is a local search optimization method for gradient-based learning. It is used to solve a

546 complex nonlinear problem, and the network weight is determined via a local
547 improvement using gradual adjustments. The algorithm may fall into a local
548 extremum, and the weight may converge to a local minimum. When this occurs, it
549 leads to a failure of the network training, and the estimation errors for the capacity
550 degradation may have singularities. As a result, the estimated capacity degradation
551 can be relatively large (Fig. 9). Furthermore, the number of iterations has an apparent
552 influence on training time, which becomes inevitably long. However, the ELM has a
553 simple structure, learns quickly, and has generally good performance. The input of
554 weights and hidden layer biases in the ELM can be randomly assigned, and the ELM
555 can be determined well analytically with a simple generalized inverse operation [24].
556 In other words, the ELM tends to reach the solutions in a straightforward manner
557 without encountering trivial issues. Therefore, the ELM learning algorithm appears to
558 be much simpler than the traditional BP neural networks in terms of the estimation
559 accuracy and learning speed. Also, the results for multiple training are the same, and
560 because of the essential characteristics of the ELM, the time required shows little
561 change. Therefore, the advantages of the extracted HIs and ELM are advantageous for
562 online implementation of the proposed framework for SoH estimation for EVs.

563 # 5. Conclusions and future work

564 A synergy of multiple HIs with an ELM has been exploited to synthesize a joint
565 model-based and ELM-oriented framework for online SoH estimation. The main
566 conclusions in this paper are as follows:

567 (1) A large amount of testing data at different temperatures using multiple cells
568 with identical chemistry was used to verify the performance of the joint framework.

569 (2) The extracted multiple HIs using a dynamic loading profile were immune to

different dynamic loading profiles, and they were used as the input for the estimator to characterize the capacity degradation. The extracted HIs can be rapidly and efficiently calculated for realistic EV operation, and the HIs are proven on the basis of different correlation analyses to be effective for estimating SoH.

(3) The ELM was introduced in the development of a joint model-based and ELM-oriented framework for online SoH estimation. The ELM learns quickly and has a high degree of estimation accuracy. The developed framework was very effective and robust with a maximum estimation error less than 2.5%. Also, from multiple perspectives (including operation time and estimation accuracy), the ELM-oriented SoH estimation approach produces better results than the traditional BP neural network.

In future work, additional issues will be considered. First, the low temperature effect on the resistance will be considered. Thus far, only the SoH of the cells that comprise the battery pack of an EV have been addressed. Because the pack consists of serial and parallel cells, we will also study how we can extend the approach we present herein for use with an EV pack.

6. Acknowledgements

This work was supported by the National Natural Science Foundation of China (Grant No.51267002, Grant No.51667006), Guangxi Key Laboratory of Manufacturing System & Advanced Manufacturing Technology (Grant No.15-140-30S002), Innovation Project of Guangxi Graduate Education (Grant No.YCSW2017038), and Guangxi Natural Science Foundation (Grant No.2015GXNSFAA139287).

7. References

[1] Zhou L, Zheng Y, Ouyang M, Lu L. A study on parameter variation effects on battery packs for electric vehicles. J Power Sources. 2017;364:242-52.

[2] Li X, Wang Z. A novel fault diagnosis method for lithium-Ion battery packs of electric vehicles. Measurement. 2018;116:402-11.

[3] You GW, Park S, Oh D. Real-time state-of-health estimation for electric vehicle batteries: A data-driven approach. Appl Energ. 2016;176:92-103.

[4] Berecibar M, Gandiaga I, Villarreal I, Omar N, Van Mierlo J, Van den Bossche P. Critical review of state of health estimation methods of Li-ion batteries for real applications. Renewable and Sustainable Energy Reviews. 2016;56:572-87.

[5] Hu X, Jiang J, Cao D, Egardt B. Battery Health Prognosis for Electric Vehicles Using Sample Entropy and Sparse Bayesian Predictive Modeling. Ieee T Ind Electron. 2016;63(4):2645-56.

[6] Ungurean L, Cârstoiu G, Micea MV, Groza V. Battery state of health estimation: a structured review of models, methods and commercial devices. Int J Energ Res. 2017;41(2):151-81.

[7] Haifeng D, Xuezhe W, Zechang S,'Presented at' 2009 IEEE Vehicle Power and Propulsion Conference,0007-10-20,2009.

[8] Bi J, Zhang T, Yu H, Kang Y, Yan J. State-of-health estimation of lithium-ion battery packs in electric vehicles based on genetic resampling particle filter. Appl Energ. 2016;182:558-68.

[9] Waag W, Fleischer C, Sauer DU. Critical review of the methods for monitoring of lithium-ion batteries in electric and hybrid vehicles. J Power Sources. 2014;258:321-39.

[10] Christensen J, Newman J. A Mathematical Model for the Lithium-Ion Negative Electrode Solid Electrolyte Interphase. J Electrochem Soc. 2004;151(11):A1977-88.

[11] Ngoc-Tham T, Khan AB, Choi W. State of Charge and State of Health Estimation of AGM VRLA Batteries by Employing a Dual Extended Kalman Filter and an ARX Model for Online Parameter Estimation. Energies. 2017;10(1371).

[12] Kim IS. A Technique for Estimating the State of Health of Lithium Batteries Through a Dual-Sliding-Mode Observer. Ieee T Power Electr. 2010;25(4):1013-22.

[13] Shen P, Ouyang M, Lu L, Li J, Feng X. The Co-estimation of State of Charge, State of Health, and State of Function for Lithium-Ion Batteries in Electric Vehicles. Ieee T Veh Technol. 2018;67(1):92-103.

[14] Nuhic A, Terzimehic T, Soczka-Guth T, Buchholz M, Dietmayer K. Health diagnosis and remaining useful life prognostics of lithium-ion batteries using data-driven methods. J Power Sources. 2013;239:680-8.

[15] Zhou Y, Huang M, Chen Y, Tao Y. A novel health indicator for on-line lithium-ion batteries remaining useful life prediction. J Power Sources. 2016;321:1-10.

[16] Tong S, Klein MP, Park JW. On-line optimization of battery open circuit voltage for improved state-of-charge and state-of-health estimation. J Power Sources. 2015;293:416-28.

[17] Chen L, Lin W, Li J, Tian B, Pan H. Prediction of lithium-ion battery capacity with metabolic grey model. Energy. 2016;106:662-72.

[18] Liu D, Zhou J, Liao H, Peng Y, Peng X. A Health Indicator Extraction and Optimization Framework for Lithium-Ion Battery Degradation Modeling and Prognostics. IEEE Transactions

on Systems Man & Cybernetics Systems. 2015;45(6):915-28.

[19] Liu D, Wang H, Peng Y, Xie W, Liao H. Satellite Lithium-Ion Battery Remaining Cycle Life Prediction with Novel Indirect Health Indicator Extraction. Energies. 2013;6(8):3654-68.

[20] Hu X, Li SE, Jia Z, Egardt B. Enhanced sample entropy-based health management of Li-ion battery for electrified vehicles. Energy. 2014;64:953-60.

[21] Yang F, Wang D, Zhao Y, Tsui KL, Bae SJ. A study of the relationship between coulombic efficiency and capacity degradation of commercial lithium-ion batteries. Energy. 2018;145:486-95.

[22] Goh T, Park M, Seo M, Kim JG, Kim SW. Capacity estimation algorithm with a second-order differential voltage curve for Li-ion batteries with NMC cathodes. Energy. 2017;135:257-68.

[23] Zhang K, Luo M. Outlier-robust extreme learning machine for regression problems. Neurocomputing. 2015;151(3):1519-27.

[24] Huang G, Zhu Q, Siew C. Extreme learning machine: Theory and applications. Neurocomputing. 2006;70(1-3):489-501.

[25] Zou Y, Hu X, Ma H, Li SE. Combined State of Charge and State of Health estimation over lithium-ion battery cell cycle lifespan for electric vehicles. J Power Sources. 2015;273:793-803.

[26] Xiong R, He H, Sun F, Zhao K. Evaluation on State of Charge Estimation of Batteries With Adaptive Extended Kalman Filter by Experiment Approach. Ieee T Veh Technol. 2013;62(1):108-17.

[27] Tulpule P, Marano V, Rizzoni G,Effects of Different PHEV Control Strategies on Vehicle Performance,2009.

[28] Chen L, Lü Z, Lin W, Li J, Pan H. A new state-of-health estimation method for lithium-ion batteries through the intrinsic relationship between ohmic internal resistance and capacity. Measurement. 2018;116:586-95.

[29] Saha B, Goebel K, Poll S, Christophersen J,An integrated approach to battery health monitoring using bayesian regression and state estimation,2007.

[30] Zhe L. Characterization Research of LiFePO4 Batteries for Application on Pure Electric Vehicles: Tsinghua University, 2011.

[31] Guo Z, Wu J, Lu H, Wang J. A case study on a hybrid wind speed forecasting method using BP neural network. Knowl-Based Syst. 2011;24(7):1048-56.

[32] Dubarry M, Svoboda V, Hwu R, Liaw BY. Capacity and power fading mechanism identification from a commercial cell evaluation. J Power Sources. 2007;165(2):566-72.

[33] Barré A, Deguilhem B, Grolleau S, Gérard M, Suard F, Riu D. A review on lithium-ion battery ageing mechanisms and estimations for automotive applications. J Power Sources. 2013;241(11):680-9.

Highlights

Multiple health indicators are extracted online for battery degradation modeling

Multiple correlation analyses are utilized to illustrate the health indicators performance

A joint model-based and ELM-oriented framework for online SoH estimation is developed

The SoH is estimated effectively with less than 2.5% maximum error